Indian Journal of Chemical Technology
Vol. 31, November 2024, pp. 829-839
DOI: 10.56042/ijct.v31i6.12514

Numerical analysis of thermal behaviour on MHD hybrid nanofluid flow over a radially convective stretching surface

M. Ragavi [1], P. Sreenivasulu [2] & T. Poornima [1]*

[1]Department of Mathematics, School of Advanced Sciences, Vellore Institute of Technology, Vellore-632014, India

[2]Department of Mathematics, Sri Venkateswara College of Engineering, Tirupati - 517507, India

*E-mail: poornima.t@vit.ac.in

Received 16 July 2024; accepted 21 November 2024

Incorporation of viscous dissipation and convective thermal exchange collectively enhances the performance and ensures high product quality in industrial processes like polymer extrusion. The current study examines the time-dependent movement and thermal characteristics of an electrically conducting hybrid nanofluid (Au-Cu/H_2O) over a surface stretching radially in a porous medium, accounting for slip and dissipation due to friction. The analysis considers the influence of heat source and heat convection at the boundary. The flow-controlling partial differential equations are converted to ordinary differential equations by incorporating similarity transformations. Using the MATLAB bvp4c solver, a numerical solution for velocity and temperature distribution is obtained. The advantages of the current model include improved cooling efficiency, reduced risk of overheating, and energy conservation. The present research shows significant consistency with previous research**.** The notable observations of this study indicate that velocity slip, magnetic parameter, and porosity characteristics tend to reduce velocity distributions. Higher values of the Biot number, magnetic field, and Eckert number lead to improved thermal dispersions. In addition to this numerical technique, we leverage a statistical technique involving multiple linear regression analysis to examine thermal transfer and the skin friction coefficient.

Keywords: Convective heat transfer, Hybrid nanofluid, MHD, Ohmic heating, Radial stretching, Viscous dissipation

Introduction

Heat transmission processes have captured interest in various fields due to their use in engineering and industrial projects. It is essential for designing efficient heating and cooling systems. In recent years, nanofluids have garnered enhanced cooling and condensing efficiencies by controlling attributes. Nanofluids are colloidal nanoparticle suspensions in a base fluid. It has shown remarkable enhancements in thermal conductivity and heat transfer properties. Choi *et al.*[1] was the first to observe a notable augmentation when non-metal or metal particles merge with fluid. Rashidi *et al.*[2] discussed controlling thermophysical attributes by nanoparticle volume fraction and migration. Jedi *et al.*[3] employed statistical modelling techniques to analyze the flow of nanofluid over a stretching sheet. Khan *et al.*[4] investigated the characteristics of a time-dependent electrically conducting Williamson nanofluid motion near a stretching surface.

Sreedevi *et al.*[5] explored how electrically conducting fluid moves unevenly with thermal and mass diffusion across an extending sheet. Kumbhakar and Nandi[6] inquired into the dynamics of a hydromagnetic hybrid nanofluid near a nonlinear permeability-extending sheet, taking into account the impact of non-linear thermal radiation. Furthermore, they conducted a regression analysis to investigate the correlation between skin friction and the Nusselt number. Their solution is highly efficient for cooling processes and cosmetics. Alkasabeh[7] examined the thermal conduction of a Casson hybrid nanofluid as it moved across a vertically extending sheet under the influence of a magnetic field. The Chebyshev differential quadrature method was utilized to find a numerical solution. A study by Misha *et al.*[8] examined how hybrid nanofluids (HNFs) move across a surface, taking into account both chemical reactions and the influence of suction and injection. This study offers valuable insights into thinning and thickening polymeric sheets in the chemical industry. Awan *et al.*[9] examined the Ellis hybrid nanofluid flow model around an extending cylinder under the influence of a magnetic field.

Magnetohydrodynamics (MHD) is the study of how heat moves through a system by looking at the

motion of a fluid that can conduct electricity and is surrounded by a magnetic field. Waini *et al.*[10] examined the continuous fluid movement and transmission of heat in a mixture of Cu-Al_2O_3 nanoparticles. The study focuses on how this nanofluid behaves while flowing across a surface that may either stretch or contract in the presence of radiation. Khan *et al.*[11] looked into how a magnetized hybrid nanofluid moves across a sheet that is progressively stretching and shrinking. The fluid moves with a heat source and sink. Roseli *et al.*[12] scrutinized the consequence of slippage on the boundary layer characteristics of an electrically conducting stagnation point flow with thermal transfer in a porous medium over a sheet that can be contracted/stretched and exhibit dual layering. They also investigated the potential for improved control over boundary layer flow with velocity slip. Considering thermal slip, Abbas *et al.*[13] investigated non-Newtonian Maxwell nanofluid flow across a stretched sheet in a porous medium. Revathi and Poornima [14] studied a Sutterby nanoflow model as it passed over a stretched sheet implanted in an absorbent medium. The proposed concept finds application in various thermal management systems, including heat exchangers, electronic cooling devices, and radiators. Patil *et al.*[15] explored the mass transfer and heat transport of a Williamson nanofluid influenced by a magnetic field flowing past a porous expanding surface with the inclusion of thermal radiation effects and chemical interactions. This study is relevant to various fluid processes, including food processing, oil extraction, and glass manufacturing.

The passage of electric current through a conductor (solids or liquids) encounters resistance, which leads to the conversion of electrical energy into heat (thermal energy). This phenomenon is known as Joule heating or Ohmic heating. In this scenario, collisions with free electrons transfer energy. Ullah *et al.*[16] conducted a study on the time-dependent flow of a nanoparticle suspension influenced by a magnetic field confined between parallel plates. The optimum auxiliary function technique (OAFM) analytically addressed the resulting boundary value issue. The OAFM method yields precise outcomes while requiring little computing effort. Ali and Alim[17] analyzed the significance of the velocity slip, Joule heating effect, and viscous energy dissipation on the MHD boundary layer flow of a nanofluid past a wedge-shaped porous surface. Their findings contribute to a better understanding of mass and thermal transport processes. Joyce *et al.*[18] looked at what happened to a porous stretched sheet when hybrid nanofluid (Cu-Al_2CO_3/water) went through it. The study focuses on assessing the rate of entropy creation and fluid behavior in various situations. A study by Riaz *et al.*[19] looked into how a mixed-mode convection nanofluid flows across a stretched surface, including the effects of heat source/sink, viscous dissipation, and joule heating.

Convective heat exchange across a stretching surface plays a crucial role in various industrial and engineering processes. Kamran[20] analysed the influence of thermal sources, viscous heating, and heat sinks on the mixed convective flow of a micropolar liquid over a porous sheet undergoing stretching or shrinking. Their findings could prove beneficial in fields such as crystal growth, artificial heart valve polishing, and addressing internal cavities. Kumar and Poonia[21] conducted an extensive investigation of the flow characteristics of MHD nanofluid containing ethylene glycol and copper nanoparticles through an exponentially stretched sheet. Ashraf *et al.*[22] examined the motion of a nanofluid containing a mixture of different nanoparticles past a curved surface. Their analysis took into account the influence of velocity slip and convective heat boundary conditions. The findings have practical implications for enhancing heat transfer in various engineering applications. Sravan Kumar [23] studied the impact of a hybrid nanofluid (Cu-Fe_3O_4/Ethylene Glycol) on physical quantities in natural convective flow over a stretching surface. Saini *et al.*[24] explored the axis symmetric movement of a non-Newtonian Williamson fluid, which changes over time due to an outward stretching surface. Resources for studying the movement of nanofluid near a surface under radial stretching are available in references[25-33].

A critical review of the literature reveals no prior studies investigating the flow and thermal characteristics of hybrid nanofluid (Au-Cu/H_2O) over a radially stretching surface using a bvp4c technique (numerical) and multiple linear regression approach (statistical). This research explores the interplay between a thermal source and viscous dissipation on the flow behavior of a time-dependent electrically conducting hybrid nanofluid past a heat-exchanging surface under velocity slip conditions. The governing partial differential equations have

been simplified into a set of ordinary differential equations by utilizing appropriate similarity transformations. Further, we employ the bvp4c solver using MATLAB software to solve these equations numerically. This inquiry aims to explore the following research questions using numerical and statistical methodologies:

I. What are the reasons for changing velocity and thermal distribution in response to various flow control parameters, including heat source, magnetic field strength, porosity characteristics, Biot number, and Eckert number?
II. In what ways do the relevant parameters affect the Nusselt number and skin friction coefficient?
III. How can we analyze and understand physical quantities using multiple linear regression?

Various graphs and tables effectively display the numerical findings. We conducted a thorough comparison of our findings with those previously published in the literature to ensure the accuracy and validity of the selected numerical method. The current model offers several benefits, including enhanced cooling efficiency and energy conservation.

Mathematical Model

An electrically charged, unsteady 2D hybrid nanofluid (Au-Cu/H_2O) passing a convective, radially stretched surface immersed in a porous medium has been taken into consideration. The sheet is positioned in the $z = 0$ plane, indicating the presence of fluid in the $z > 0$ region. We employed the cylindrical polar framework (r, θ, z) to offer an accurate mathematical depiction. Fig. 1 shows the flow configuration and physical model. The following are some of the assumptions that we have made to effectively carry out the current investigation.

- The sheet undergoes radial stretching with a velocity $U_w = \frac{qr}{1-\epsilon t}$, where q and ϵ are small physical parameters related to the unsteady stretching surface.
- An inconsistent transverse magnetic flux density $B = \frac{B_0}{\sqrt{1-\epsilon t}}$ is applied in z-direction.
- Joule heating (due to electrical resistance) and viscous dissipation (due to friction) effects have been incorporated into the analysis.

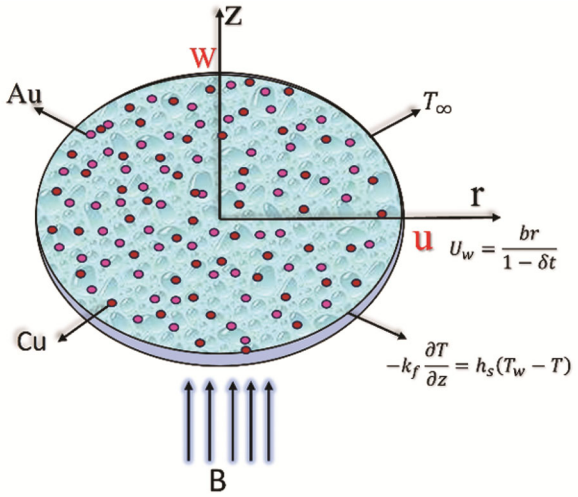

Fig. 1 — Physical model of the problem

- The temperature and velocity fields are represented by the forms T=T (r, z, t) and v = [u (r, z, t), 0, w (r, z, t)].
- The fluid temperature can be described by the form $T = T_w = T_\infty + \frac{br}{1-\epsilon t}$, where T_w represents the temperature of the wall and T_∞ denotes the thermal situation in a free stream.

Given the assumption stated above, the governing equation for the current problem can be formulated as follows Hayat *et al.*[29]:

Continuity equation

$$\frac{\partial u}{\partial r} + \frac{u}{r} + \frac{\partial w}{\partial z} = 0 \quad \ldots(1)$$

Momentum equation

$$\frac{\partial u}{\partial t} + u\frac{\partial u}{\partial r} + w\frac{\partial u}{\partial z} = \frac{\mu_{hnf}}{\rho_{hnf}}\frac{\partial^2 u}{\partial z^2} - \frac{\sigma_{hnf}B^2 u}{\rho_{hnf}} - \frac{\mu_{hnf}}{\rho_{hnf}}\frac{u}{k^*} \quad \ldots(2)$$

Energy equation

$$\frac{\partial T}{\partial t} + u\frac{\partial T}{\partial r} + w\frac{\partial T}{\partial z} = \frac{k_{hnf}}{(\rho C_p)_{hnf}}\frac{\partial^2 T}{\partial z^2} + \frac{\mu_{hnf}}{(\rho C_p)_{hnf}}\left(\frac{\partial u}{\partial z}\right)^2 + \frac{\sigma_{hnf}B^2u^2}{(\rho C_p)_{hnf}} + \frac{Q_0}{(\rho C_p)_{hnf}}(T - T_\infty) \quad \ldots(3)$$

and the conditions at the boundary are[31-32]

$$u = U_w + A_1\frac{\partial u}{\partial z}, w = 0, -k_f\frac{\partial T}{\partial z} = h_s(T_w - T) \text{ at z=0}$$
$$u \to u_\infty, T \to T_\infty \text{ as z}\to \infty \quad \ldots(4)$$

Hybrid nanofluid thermophysical characteristics are described as follows[35]

$$\frac{\mu_{hnf}}{\mu_f} = \frac{1}{(1-\epsilon_1)^{2.5}(1-\epsilon_2)^{2.5}}$$

$$\rho_{hnf} = (1-\epsilon_2)\left[(1-\epsilon_1)\rho_f + \epsilon_1\rho_{s1}\right] + \epsilon_2\rho_{s2}$$

$$\left(\rho C_p\right)_{hnf} = (1-\epsilon_2)\left[(1-\epsilon_1)\left(\rho C_p\right)_f + \epsilon_1\left(\rho C_p\right)_{s1}\right] + \epsilon_2\left(\rho C_p\right)_{s2}$$

$$\frac{k_{hnf}}{k_f} = \frac{k_{s2}+2k_{bf}-2\delta_2(k_{bf}-k_{s2})}{k_{s2}+2k_{bf}+\delta_2(k_{bf}-k_{s2})} \times \frac{k_{s1}+2k_f-2\delta_1(k_f-k_{s1})}{k_{s1}+2k_f+\delta_1(k_f-k_{s1})}$$

$$\frac{\sigma_{hnf}}{\sigma_f} = \left(1+\frac{3\left(\frac{\sigma_{s2}}{\sigma_f}-1\right)\epsilon_2}{\left(\frac{\sigma_{s2}}{\sigma_f}+2\right)-\left(\frac{\sigma_{s2}}{\sigma_f}-1\right)\epsilon_2} \times 1 + \frac{3\left(\frac{\sigma_{s1}}{\sigma_f}-1\right)\epsilon_1}{\left(\frac{\sigma_{s1}}{\sigma_f}+2\right)-\left(\frac{\sigma_{s1}}{\sigma_f}-1\right)\epsilon_1}\right) \quad \ldots(5)$$

The velocity slip factor is represented by $A_1 = A\sqrt{1-\epsilon t}$. The variables ϵ_1 and ϵ_2 refer to the volume fraction of *Au* and *Cu* nanoparticles. This study uses the following abbreviations: *hnf* for the hybrid nanofluid, *s1* for the first solid nanoparticle (gold), *s2* for the second solid nanoparticle (copper), and *f* for the working fluid. Table 1 lists the thermophysical properties of the working fluid and nanoparticles.

Solution of the problem

Our problem involves coupled partial differential equations. So, the similarity variables are utilized to transform the mathematical model into dimensionless forms.

The similarity transformation used in this study is demonstrated as follows by Azam *et al*.[33]

$$\psi = \frac{-r^2\sqrt{q\nu_f}}{\sqrt{1-\epsilon t}} f(\eta)$$
$$\eta = \mathrm{z}\sqrt{\frac{q}{\nu_f(1-t\epsilon)}} \quad \ldots(6)$$
$$\theta(\eta) = \frac{T-T_\infty}{T_w-T_\infty}$$

Now in terms of stream function ψ, the velocity components of transverse and longitudinal aspects are defined by

Table 1 — Properties of nanoparticles (Au, Cu) and base fluid (H_2O) [34].

Physical characters	Au	Cu	H_2O
K (*W/mk*)	318	400	0.613
$\Sigma\,(\Omega m)^{-1}$	4.1×10^6	59.6×10^6	0.05
C_p (*J/kgk*)	129	385	4179
P (kg/m^3)	19300	8933	997.1

$$u = \frac{1}{r}\frac{\partial\psi}{\partial z} = U_w f'(\eta),$$
$$w = \frac{-1}{r}\frac{\partial\psi}{\partial r} = -2\sqrt{\frac{q\vartheta}{1-\epsilon t}} f(\eta). \quad \ldots(7)$$

which satisfies the continuity equation (Eq. (1)).

The non-dimensional form of the energy equation and momentum equation can be obtained through the utilization of the similarity transformations.

$$P_1 f''' + 2ff'' - (f')^2 - U_s\left(f' + \frac{\eta}{2}f''\right) - P_2 M_g f' - P_1 D_p f' = 0, \quad \ldots(8)$$

$$\frac{P_3\theta''}{Pr} + 2f\theta' - f'\theta + P_4 E_N (f'')^2 - U_s\left(\theta + \frac{\eta}{2}\theta'\right) + P_5 M_g E_N (f')^2 + H_s\theta = 0, \quad \ldots(9)$$

$$f(\eta) = 0, f'(\eta) = 1 + S_p f''(\eta), \theta'(\eta) = -B_N\left(1-\theta(\eta)\right) \text{ at } \eta = 0,$$
$$f'(\eta) \to 0, \theta(\eta) \to 0 \text{ as } \eta \to \infty. \quad \ldots(10)$$

The variables $P_1, P_2, P_3, P_4 and\ P_5$ in the equation shown above is explicitly defined as follows:

$$P_1 = \frac{\mu_{hnf}/\mu_f}{\rho_{hnf}/\rho_f},\ P_2 = \frac{\sigma_{hnf}/\sigma_f}{\rho_{hnf}/\rho_f},$$

$$P_3 = \frac{k_{hnf}/k_f}{(\rho C_p)_{hnf}/(\rho C_p)_f},\ P_4 = \frac{\mu_{hnf}/\mu_f}{(\rho C_p)_{hnf}/(\rho C_p)_f},\ P_5 = \frac{\sigma_{hnf}/\sigma_f}{(\rho C_p)_{hnf}/(\rho C_p)_f}.$$

Here are several dimensionless constants: $E_N = \frac{U_w^2}{C_p(T-T_\infty)}$; $D_P = \frac{(1-\epsilon t)\mu_f}{\rho_f q k^*}$; $U_s = \frac{\epsilon}{q}$; $Pr = \frac{\rho C_p \nu_f}{k_f}$; $M_g = \frac{B_0^2\sigma_f}{q\rho_f}$; $S_p = A\sqrt{\frac{U_w\nu_f}{r}}$; $Re = \frac{rU_w}{\nu_f}$, $H_s = \frac{Q_0}{q(\rho C_p)}$; $B_N = \frac{h_s}{k}\sqrt{\frac{\nu_f}{q}}$.

Engineering-relevant physical quantities

The fundamental physical parameters for the governing flow problem are the local shear rate (C_f) and Nusselt number (Nu), designated by Khashi *et al*.[35]

$$C_f = \frac{\tau_w}{\rho_f {U_w}^2}, Nu = \frac{rq_w}{K_f(T_w-T_\infty)}. \quad \ldots(11)$$

$$\tau_w = \mu_{hnf}\left[\frac{\partial u}{\partial z}\right], and\ q_w = -k_{hnf}\frac{\partial T}{\partial z} \text{ at } z = 0.$$

The values illustrated above represent the shear rate coefficient and heat flux at the boundary. Eq. (11) can be simplified into a non-dimensional form as follows:

$$C_f\sqrt{Re} = \frac{\mu_{hnf}}{\mu_f} f''(0),$$
$$Re^{-1/2}Nu = -\frac{k_{hnf}}{k_f}\theta'(0). \quad \ldots(12)$$

Execution of Numerical technique

Due to the high nonlinearity and coupled terms found in the mathematical model seen in Eqs (8) and (9) as well as the boundary conditions (10), it is difficult to solve directly. Therefore, the system of the equation is solved numerically by employing the bvp4c solver (a well-defined finite difference method) in MATLAB software. Using the substitutions $f = g$ (1), $f' = g$ (2), $f'' = g$ (3), $\theta = g$ (4), and $\theta' = g$ (5), the higher-order equation is recast as a set of first-order equations.

The specific procedure is outlined below:

$$f' = g(2)$$
$$f'' = g(3)$$
$$f''' = \Big[MP_2 g(2) + (g(2))^2 + D_p P_1 g(2) + U_s\left(g(2) + \frac{\eta}{2}g(3)\right) - 2g(1)g(3)\Big]\frac{1}{P_1}$$
$$\theta' = \left[g(2)g(4) - P_4 E_N\big(g(3)\big)^2 - 2g(1)g(5) + U_s\left(g(4) + \frac{\eta}{2}g(5)\right) - P_5 M_g E_N\big(g(2)\big)^2 - H_s g(4)\right]\frac{Pr}{P_3}$$

The boundary conditions are listed as follows:

$$g_1(0) = 0,\ g_2(0) = \big[1 + S_p g_3(0)\big],$$
$$g_2(\infty) \to 0,\ g_5(0) = -B_N[1 - g_4(0)],$$
$$g_4(\infty) \to 0.$$

This technique employs the shooting approach to identify missed initial conditions, leading to faster processing times. To satisfy the boundary criteria, a crucial step involves choosing a specific value for η at infinity. As a result, the majority of our activities are performed using various values. It is essential to determine the boundary conditions for all parameter values. An accuracy criterion of 10^{-5} is taken in this study.

Results and Discussion

This section discusses the influence of many relevant factors on the velocity and thermal distribution throughout the surface. To perform computations, certain non-dimensional parameters have been taken into account. These parameters include the local Biot number (B_N=0.5), porosity parameter (D_p=0.5), unsteadiness parameter (U_s=0.2), magnetic parameter (M_g=0.2), Prandtl number (Pr=6.2), slip parameter (S_p=0.5) and Eckert number (E_N=0.04), heat source parameter (H_s=0.3). Except for the different values shown in relevant figures and tables, these numerical values were constant during the theoretical investigation. Furthermore, we conduct a thorough analysis of the computational outcomes for the skin friction coefficient (which represents the wall shear stress) and the Nusselt number (which represents the wall thermal flux). The bvp4c solver in MATLAB is utilized to obtain numerical solutions. In order to assess the reliability and precision of our numerical findings, we conducted a comparison with the published results of Makinde *et al.*[32]. Our results exhibited a remarkable level of agreement with their results, as seen in Table 2.

Effects on velocity distribution

The velocity distribution completely determines the fluid flow onto a particular surface. Changes in fluid movement can be caused by various external forces, such as magnetic fields. Fig. 2 depicts a decreasing trend in flow distribution as the magnetic parameter (M_g) increases. The existence of a magnetic field induces a resistive force known as the Lorentz force, which acts to considerably impede the velocity of the fluid. Fig. 3 portrays the influence of porosity (D_p) on $f'(\eta)$(velocity profile). The reduction in velocity distribution is a consequence of increasing the porosity, which occurs as a result of the existence of the permeable medium. Normally, the porosity component has a propensity to absorb a substantial volume of fluid from the boundary layer, causing a decrease in the velocity profile over the whole flow domain. Fig. 4 illustrates the influence of the

Table 2 — Comparison of skin friction coefficient when $S_p = D_p = \epsilon_1 = \epsilon_2 = 0$

M_g	Makinde et al. [32]	Current result
0	-1.17372	-1.17372
0.5	-1.36581	-1.36581
1	-1.53571	-1.53571
2	-1.83049	-1.83049

unsteadiness parameter. The velocity profile shows a decreasing trend as the unsteadiness parameter increases. Disruptions impede the uninterrupted flow of the fluid, resulting in a decrease in velocity. Fig. 5 depicts the impact of the slip parameter denoted as S_p

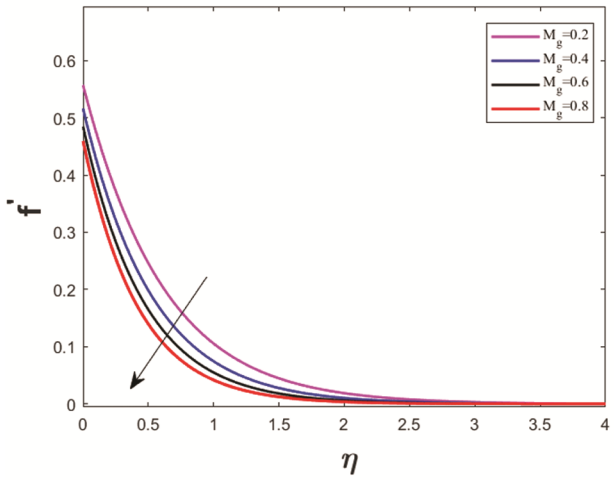

Fig. 2 — Implication of M_g on velocity (0.2, 0.4, 0.6, 0.8)

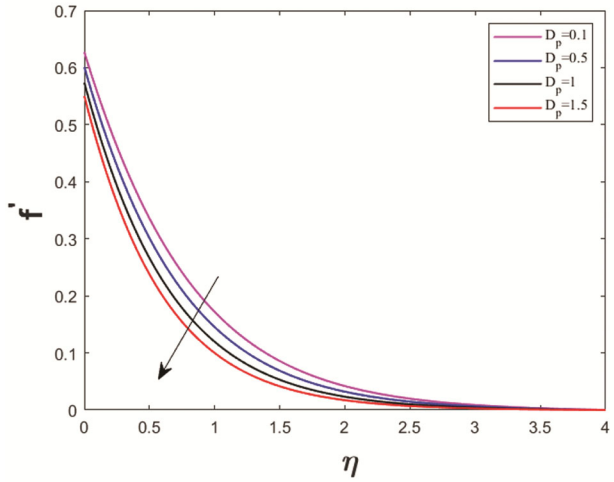

Fig. 3 — Implication of D_p on velocity (0.1, 0.5, 1.0, 1.5)

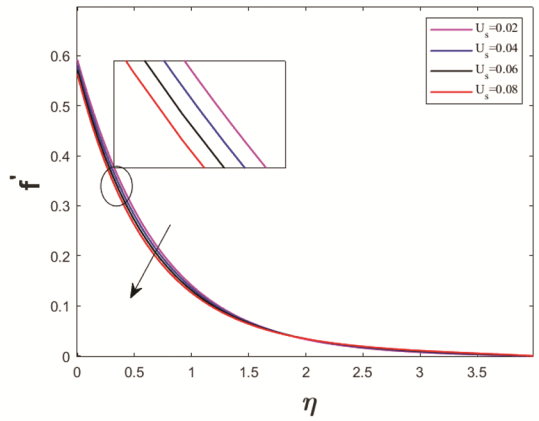

Fig. 4 — Implication of U_s on velocity (0.02, 0.04, 0.06, 0.08)

on flow distribution. We observe that an increase in S_p leads to a decrease in the thickness of the momentum boundary layer, thereby reducing fluid flow. This is because as the slip factor increases, the velocity difference between the surface and the fluid increases, leading to a reduced interaction between the surface and the fluid flow.

Effects on thermal distribution

According to the data presented in Fig. 6, the temperature profile increases gradually as the magnetic parameter (M_g) increases. This is due to the magnetic force generating resistance among the fluid particles, which produces thermal energy within the boundary layer and a subsequent temperature rise. Enhancing the Eckert number (E_N) increases the thermal distribution, as shown in Fig. 7. In general, there is a correlation between enthalpy and kinetic energy. Viscosity facilitates the completion of work

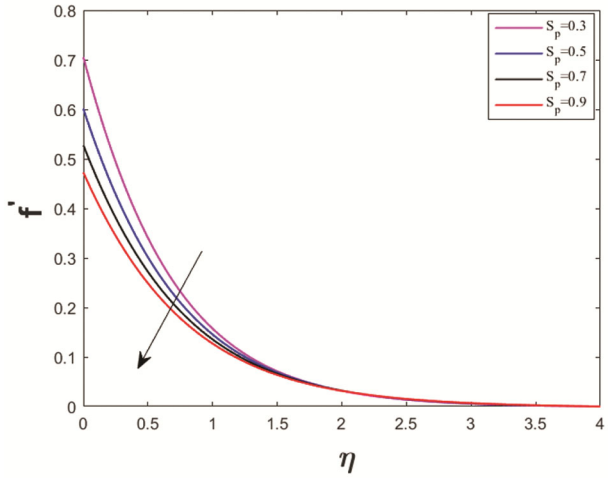

Fig. 5 — Implication of S_p on velocity (0.3, 0.5, 0.7, 0.9)

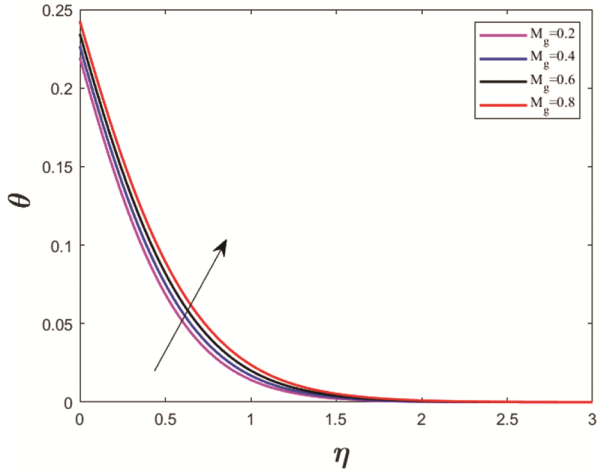

Fig. 6 — Implication of M_g on temperature (0.2, 0.4, 0.6, 0.8)

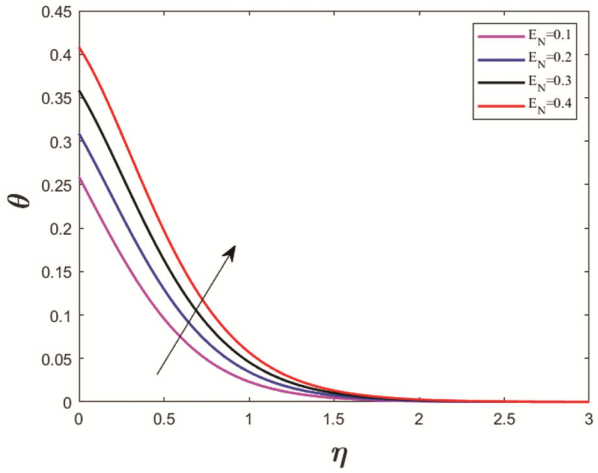

Fig. 7 — Implication of E_N on temperature (0.1, 0.2, 0.3, 0.4)

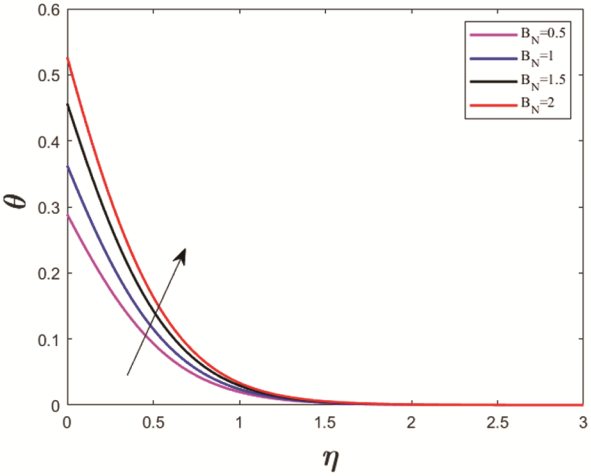

Fig. 8 — Implication of B_N on temperature (0.5, 1.0, 1.5, 2.0)

by transforming the kinetic energy of fluid into internal energy. This process is known as viscous dissipation, which can elevate the temperature of fluid. Fig. 8 illustrates the effects of B_N on the thermal profile. Based on the investigation, we demonstrate that the dimensionless thermal distribution increases in direct proportion to the increase in B_N (Biot number). Increased convection strength results in higher surface temperatures, which in turn allows for a greater thermal impact to propagate throughout the fluid. Nanofluid with convective boundary conditions provides a more suitable model than constant surface temperature settings. Fig. 9 displays the effect of H_s on thermal distribution. Therefore, energy production inside the thermal boundary layer leads to an enhancement in thermal flow profiles when H_s increases.

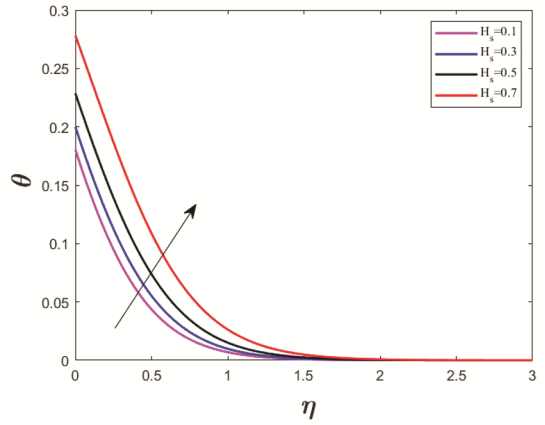

Fig. 9 — Implication of H_s on temperature (0.1, 0.3, 0.5, 0.7)

Table 3 — Variation in Skin friction coefficient

M_g	S_p	D_p	U_s	$Cf_r Re_r{}^{1}/_{2}$
0.2	0.5	0.5	0.02	-0.798551
0.4				-0.822800
0.6				-0.845303
0.8				-0.866255
	0.3			-0.983509
	0.5			-0.798551
	0.7			-0.675371
	0.9			-0.586764
		0.1		-0.747163
		0.5		-0.798551
		1		-0.853038
		1.5		-0.899191
			0.02	-0.798551
			0.04	-0.800667
			0.06	-0.802774
			0.08	-0.804872

Skin friction coefficient and Nusselt number

Tables 3 and 4 provide the numerical values of drag friction and thermal transmission rate for various values of regulating flow parameters such as slip parameter (S_p), unsteadiness parameter (U_s), porosity parameter (D_p), and magnetic parameter (M_g). According to the analysis, an increase in the values of U_s, D_p, and M_g results in a decrease in skin friction. However, the reverse behaviour is found for S_p. Based on the results, the Nusselt number increases as E_N and B_N values increase. However, the tendency reverses when the values of H_s increase. Three-dimensional surface plots in Figs. 10-12 illustrate the simultaneous effect of important factors on the heat transfer rate and skin friction. As D_p and M_g increase, the surface shear stress decreases (see Fig. 10). Fig. 11 demonstrates that the Nusselt number increases when

B_N is high, while the reverse trend is observed for E_N. In Fig. 12, we can see the impact of M_g and H_s on surface heat flux. It clarifies that the thermal transfer rate diminishes for both parameters.

Analysis of Engineering quantities using multiple linear regression

A statistical methodology known as multiple linear regression emerges as a powerful tool for delving into the interplay between a dependent variable and a set of independent variables**.** This technique empowers engineers to make predictions regarding the value of the dependent variable based on the combined influence of the independent variables. The mathematical formulation for this method can be stated as follows [36-39]:

$$y = m + m_1x_1 + m_2x_2 + m_3x_3 \dots\dots\dots + m_nx_n \quad \dots(13)$$

We use multiple regression analysis to estimate skin friction and Nusselt numbers. The estimated models have general forms, which can be expressed as:

$$Cf_{est} = m_1M_g + m_2D_p + m_3S_p + m_4U_s + m \quad \dots(14)$$

$$Nu_{est} = n_1E_N + n_2M_g + n_3U_s + n_4H_s + n_5B_N + n \quad \dots(15)$$

Here, $m_1, m_2, m_3, m_4, m, n_1, n_2, n_3, n_4, n_5$ *and* n represents the calculated regression coefficients.

It is estimated that the skin friction coefficient and Nusselt number based on different sample sizes of data. The regression coefficients for both cases are calculated using Microsoft Excel. As a result, the estimated regression models are presented in Eqs (16)-(17):

Table 4 — Variation in Nusselt Number

M_g	E_N	U_s	B_N	H_s	$Nu_rRe_r{}^{-1}/_2$
0.2	0.04	0.02	0.5	0.4	0.408964
0.4					0.404236
0.6					0.399394
0.8					0.394383
	0.1				0.393146
	0.2				0.366783
	0.3				0.340420
	0.4				0.314057
		0.02			0.415671
		0.04			0.422583
		0.06			0.428990
		0.08			0.434764
			0.5		0.528307
			1		0.676330
			1.5		0.864785
			2		1.004771
				0.1	0.428977
				0.3	0.417004
				0.5	0.398679
				0.7	0.364339

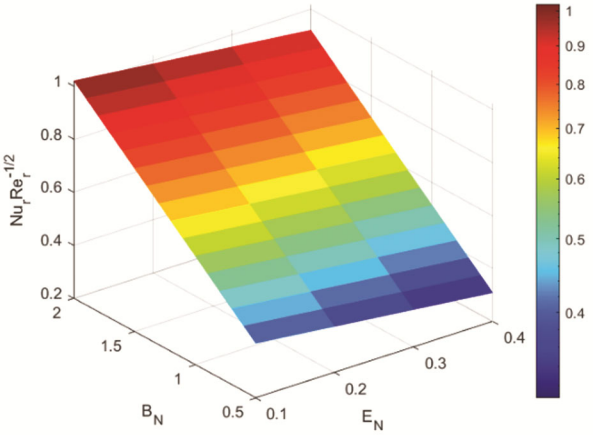

Fig. 11 — Implications of E_N and B_N on Nusselt number

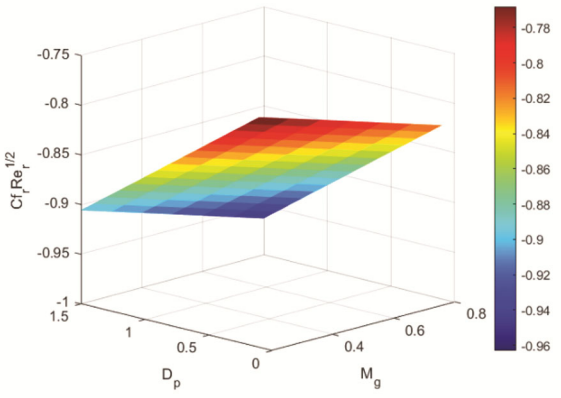

Fig. 10 — Implications of M_g and D_p on skin friction

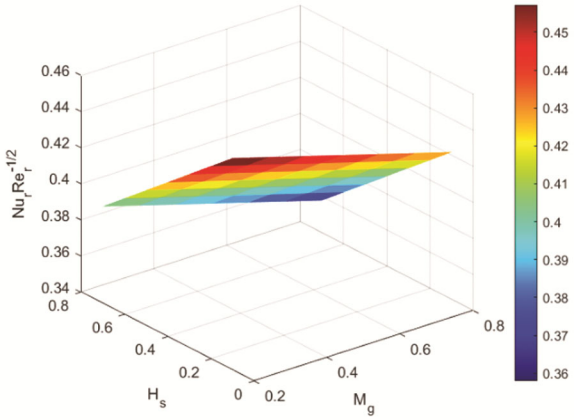

Fig. 12 — Implications of M_g and H_s on Nusselt number

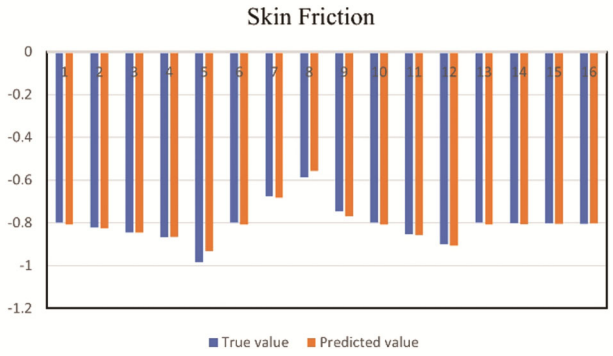

Fig. 13 — Computed versus Predicted values of Skin friction

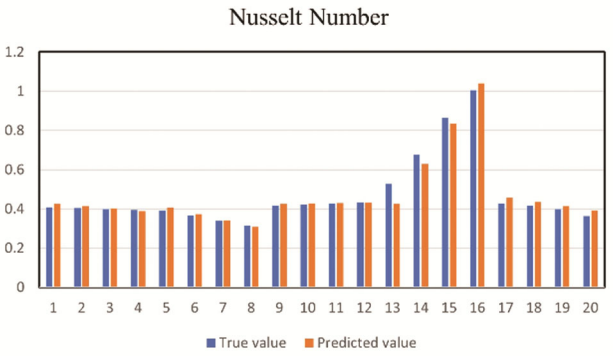

Fig. 14 — Computed versus Predicted values of Nusselt number

$$Cf_{est} = -0.09553M_g - 0.09833D_p + 0.62459S_p + 0.08520U_s - 1.05317 \quad \ldots(16)$$

$$Nu_{est} = -0.3244E_N - 0.05926M_g + 0.11702U_s - 0.10611N + 0.40973B_N + 0.28541 \quad \ldots(17)$$

The positive sign of computed regression coefficient indicates that the relevant parameter increases the skin friction coefficient or thermal transfer rate, whereas a negative sign indicates that the relevant parameter decreases the thermal transfer rate or drag coefficient. The outcomes obtained are consistent with the data presented in Tables 3 and 4. $R^2 = 0.96$ indicates that the model explains 96% of the total variation in the dependent variable. This suggests a strong fit between the model predictions and the observed data. Based on this, we can evaluate the significance and influence of various factors on the Nusselt number and skin friction coefficient, resulting in improved prediction models and insights. Figs. 13 and 14 display the concordance between the computed regression model and the selected sample data. Computed values are the numerical results obtained from solving the governing equations using the numerical method (bvp4c). Predicted values represent the outputs of the multiple linear regression model, which was developed using the true values as the dataset for training and validation. An excellent consensus exists between the real and estimated values.

Conclusion

This study investigates the behaviour and thermal transmission properties of hybrid nanofluids over an unsteady radially stretched surface, considering the impact of viscous dissipation and ohmic heating. In addition, the impacts of convective heat transfer, slip conditions, and heat sources are considered. Partial differential equations are transformed into ordinary ones through the incorporation of suitable similarity variables. Next, we use the bvp4c solver in MATLAB to get numerical solutions. Additionally, the effects of pertinent parameters on the thermal transfer rate and skin friction coefficient are evaluated through the utilization of multiple linear regression. Here is a summary of the key findings from this study:

- The distribution of velocity diminishes as local unsteadiness, porosity, and wall velocity slip parameters escalate.
- Elevating M_g (the magnetic parameter) translates to a decline in the velocity distribution, but the thermal distribution shows the opposite trend.
- The temperature profile improves as the Eckert number, heat source parameter, and Biot number increase, whereas the unsteadiness parameter shows a reverse trend.
- The predicted regression model for the skin friction is expressed as:

$$Cf_{est} = -0.09553M_g - 0.09833D_p + 0.62459S_p + 0.08520U_s - 1.05317$$

- The predicted regression model for the Nusselt number is expressed as:

$$Nu_{est} = -0.3244E_N - 0.05926M_g + 0.11702U_s - 0.10611N + 0.40973B_N + 0.28541$$

- The skin friction coefficient (surface shear stress) has a negative correlation with the porosity (D_p) and magnetic (M_g) parameters, whereas it is positively correlated with the slip parameter.
- The thermal transfer rate (Nusselt number) correlates positively with the Biot number and adversely with the Eckert number (E_N), magnetic parameter, and heat source parameter (H_s).
- Hybrid nanofluid (Au-Cu/H_2O) flow over a radially stretching surface has potential benefits in enhanced cooling efficiency and improved

system reliability. Incorporating ohmic-viscous dissipation and convection helps to improve the design of thermal cooling systems.

Nomenclature:

C_p	Specific heat at constant pressure	M_g	Magnetic parameter
K	Thermal conductivity	Nu	Nusselt number
μ	Viscosity coefficient	C_f	Skin friction coefficient
T_∞	Ambient temperature	U_s	Unsteadiness parameter
Q	Positive constant	B_N	Biot number
ϵ	Rate of stretching	E_N	Eckert number
σ	Electrical conductivity	D_P	Porosity parameter
ρ	Fluid density	Pr	Prandtl number
T_w	Surface Temperature	H_s	Heat source parameter
u, w	Velocity components along the r and z direction	Re	Reynolds number
B_0	Magnetic field strength	S_p	Slip parameter
U_w	Velocity close to the surface	$\theta(\eta)$	Non-dimensional temperature
h_s	Initial heat convection	$f'(\eta)$	Non-dimensional velocity

References

1 Choi S U S & Eastman J A, Enhancing thermal conductivity of fluids with nanoparticles, *Tech Rep Argonne National Lab*, IL (United States), (1995).

2 Rashidi S, Mahian O & Languri E M, Applications of nanofluids in condensing and evaporating systems: A review, *J Therm Anal Calorim*, 131 (2018) 2027.

3 Jedi A, Shamsudeen A, Razali N, Othman H, Zainuri N A, Zulkarnain N, Bakar N A A, Pati K D & Thanoon T Y, Statistical modeling for nanofluid flow: A stretching sheet with thermophysical property data, *Colloids Interfaces*, 4 (2020) 3.

4 Khan K A, Javed M F, Ullah M A & Riaz M B, Heat and mass transport analysis for Williamson MHD nanofluid flow over a stretched sheet, *Results Phys*, 53 (2023) 106873.

5 Sreedevi P, Sudarsana R P & Chamkha A, Heat and mass transfer analysis of unsteady hybrid nanofluid flow over a stretching sheet with thermal radiation, *SN Appl Sci*, 2 (2020) 1222.

6 Kumbhakar B & Nandi S, Unsteady MHD radiative-dissipative flow of Cu-Al_2O_3/H2O hybrid nanofluid past a stretching sheet with slip and convective conditions: A regression analysis, *Math Comput Simul*, 194 (2022) 563.

7 Alkasasbeh H, Numerical solution of heat transfer flow of Casson hybrid nanofluid over vertical stretching sheet with magnetic field effect, *CFD Lett*, 14 (2022) 39.

8 Mishra S, Swain K & Dalai R, Heat and mass transfer of water-based copper and alumina hybrid nanofluid over a stretching sheet, *Heat Transf*, 52 (2023) 1198.

9 Awan A U, Ali B, Shah S A A, Oreijah M, Guedri K & Eldin S M, Numerical analysis of heat transfer in Ellis's hybrid nanofluid flow subject to a stretching cylinder, *Case Stud Therm Eng*, 49 (2023) 103222.

10 Waini I, Ishak A & Pop I, Hybrid nanofluid flow and heat transfer over a nonlinear permeable stretching/shrinking surface, *Int J Numer Methods Heat Fluid Flow*, 29 (2019) 3110.

11 Khan A S, Xu H Y & Khan W, Magnetohydrodynamic hybrid nanofluid flow past an exponentially stretching sheet with slipconditions, *Mathematics*, 9 (2021) 3291.

12 Rozeli N S, Som A N M, Arifin N M, Ali F M & Abd-Ghani A, Double stratified MHD stagnation point slip flow over a permeable shrinking/stretching surface in a porous medium, *J Adv Res Fluid Mech Therm Sci*, 90 (2022) 64.

13 Abbas W, Megahed A M, Ibrahim M A & Said A A, Non-newtonian slippery nanofluid flow due to a stretching sheet through a porous medium with heat generation and thermal slip, *J Nonlinear Math Phys*, 30 (2023) 1221.

14 Revathi R & Poornima T, Enhanced energy transfer performance in an inclined magneto-convective sutterby ternary hybrid nanoflow: Application for nano diesel, *Contemp Mathematics*, 5(2) (2024) 1918.

15 Patil V S, Humane P P & Patil A B, MHD Williamson nanofluid flow past a permeable stretching sheet with thermal radiation and chemical reaction, *Int J Model Simul*, 43 (2023) 185.

16 Ullah H, Khan H, Fiza M, Ullah K, Islam S & Al-Mekhlafi S M, Comparative analysis of the effect of Joule heating and slip velocity on unsteady squeezing nanofluid flow, *Math Prob Eng*, 2022 (2022) 1.

17 Ali M & Alim M A, Influence of slip parameter, viscous dissipation and joule heating effect on boundary layer flow and heat transfer over a power-law stretching wedge-shaped surface with the correlation coefficient and multiple regressions, *Int J Appl Mech Eng*, 27 (2022) 1.

18 Joyce M I, Kandasamy J & Sivanandam S, Entropy generation of Cu–Al_2O_3/water flow with convective boundary conditions through a porous stretching sheet with slip effect, joule heating, and chemical reaction, *Math Comput Appl*, 28 (2023) 18.

19 Riaz S, Naheed N, Farooq U, Lu D & Hussain M, Non-similar investigation of magnetized boundary layer flow of nanofluid with the effects of Joule heating, viscous dissipation and heat source/sink, *J Magn Magn Mater*, 574 (2023) 170707.

20 Kamran M, Heat source/sink and newtonian heating effects on convective micropolar fluid flow over a stretching/shrinking sheet with slip flow model, *Int J Heat Technol*, 36 (2018) 473.

21 Kumar P & Poonia H, Slip effect on magnetohydrodynamic boundary layer flow of nanofluid over a stretching sheet with thermal radiation and thermal convective boundary condition, *Curr J Appl Sci Technol*, 41 (2022) 33.

22 Ashraf A, Zhang Z, Saeed T, Zeb H & Munir T, Convective heat transfer analysis for aluminum oxide (Al_2O_3)-and ferro (Fe_3O_4)-based nano-fluid over a curved stretching sheet, *Nanomaterials*, 12 (2022) 1152.

23 Kumar T S, Hybrid nanofluid slip flow and heat transfer over a stretching surface, *Partial Differ Equ Appl Math*, 4 (2021) 100070.

24 Saini S K, Agrawal R & Kaswan P, Activation energy and convective heat transfer effects on the radiative Williamson nanofluid flow over a radially stretching surface containing Joule heating and viscous dissipation, *Numer Heat Transf, Part A: Appl*, 85(15) (2023) 2534.

25 Shahzad A, Ali R, Hussain M & Kamran M, Unsteady axisymmetric flow and heat transfer over a time-dependent radially stretching sheet, *Alex Eng J*, 56 (2017) 35.

26 Ibrahim W & Gamachu D, Nonlinear convection flow of Williamson nanofluid past a radially stretching surface, *AIP Adv*, 9 (2019) 085026.

27 Ali B, Yu X, Sadiq M T, Rehman A U & Ali L, A finite element simulation of the active and passive controls of the MHD effect on an axisymmetric nanofluid flow with thermo-diffusion over a radially stretched sheet, *Processes*, 8 (2020) 207.

28 Jawwad A K A, Jawad M, Nisar K S, Saleem M & Hasanain B, Radiative transport of MHD stagnation point flow of chemically reacting Carreau nanofluid due to radially stretched sheet, *Alex Eng J*, 69 (2023) 699.

29 Hayat T, Qayyum S & Alsaedi A, Mechanisms of nonlinear convective flow of Jeffrey nanofluid due to nonlinear radially stretching sheet with convective conditions and magnetic field, *Results Phys*, 7 (2017) 2341.

30 Faraz F, Haider S & Imran S M, Study of magneto-hydrodynamics (MHD) impacts on an axisymmetric Casson nanofluid flow and heat transfer over unsteady radially stretching sheet, *SN Appl Sci*, 2 (2020) 1.

31 Naseem T, Shahzad A, Sohail M & Askar S, Axisymmetric flow and heat transfer in TiO_2/H_2O nanofluid over a porous stretching-sheet with slip boundary conditions via a reliable computational strategy, *Energies*, 16 (2023) 681.

32 Makinde O D, Mabood F, Khan W A & Tshehla M S, MHD flow of a variable viscosity nanofluid over a radially stretching convective surface with radiative heat, *J Mol Liq*, 219 (2016) 624.

33 Azam M, Khan M & Alshomrani A S, Effects of magnetic field and partial slip on unsteady axisymmetric flow of Carreau nanofluid over a radially stretching surface, *Results Phys*, 7 (2017) 2671.

34 Basit M A, Farooq U, Imran M, Fatima N, Alhushaybari A, Noreen S, Eldin S M & Akgül A, Comprehensive investigations of (Au-Ag/Blood and Cu-Fe_3O_4/Blood) hybrid nanofluid over two rotating disks: Numerical and computational approach, *Alex Eng J*, 72 (2023) 19.

35 Khashi N S, Waini I, Arifin N M & Pop I, Dual solutions of unsteady two-dimensional electro-magneto-hydrodynamics (EMHD) axisymmetric stagnation-point flow of a hybrid nanofluid past a radially stretching/shrinking Riga surface with radiation effect, *Int J Numer Methods Heat Fluid Flow*, 33 (2023) 333.

36 Neethu T S, Sabu A S, Mathew A, Wakif A & Areekara S, Multiple linear regression on bioconvective MHD hybrid nanofluid flow past an exponential stretching sheet with radiation and dissipation effects, *Int Commun Heat Mass Transf*, 135 (2022) 106115.

37 Revathi G, Sajja V S, Babu M J, Srinivasa B K S, Kumar A S, Raju C S K & Yook S J, Multiple linear regression analysis on the flow of ternary hybrid nanofluid by a quadratically radiated stretching surface with and second-order slip, *Waves in Random and Complex Media*, (2023) 1. Please provide volume number

38 Bhargavi N & Poornima T, Radiative impact on Jeffery trihybrid convective nanoflow over an extensible riga plate: Multiple linear regression analysis, *Contemp Math*, 5(1) (2024) 1036.

39 Kumar M D, Ahammad N A, Raju C S K, Yook S J, Shah N A & Tag S M, Response surface methodology optimization of dynamical solutions of Lie group analysis for nonlinear radiated magnetized unsteady wedge: Machine learning approach (gradient descent), *Alex Engi J*, 74 (2023) 29.